Electrocatalysis (2023) 14:473–483
https://doi.org/10.1007/s12678-023-00810-5

RESEARCH

Optimization of Ni-Mo-Coated Stainless Steel as a High-Performance Cathode in Alkaline Water Electrolysis

Mohammad Zhiani[1,2] · Mohammad Mohammadi Taghiabadi[2] · Mohammad Hassan Bagherabadi[1]

Accepted: 10 January 2023 / Published online: 30 January 2023
© The Author(s), under exclusive licence to Springer Science+Business Media, LLC, part of Springer Nature 2023

Abstract

Considering the widespread use of alkaline water electrolysis (AWE) in the chemical industry and the growing need to design and manufacture low-cost and efficient electrodes, the optimization of a Ni-Mo-coated stainless steel substrate is investigated in the present work to use this substrate as a cathode of an alkaline water electrolyzer. The crystallographic structure, surface morphology, and composition of the optimized coating are characterized by X-ray diffraction analysis (XRD), scanning electron microscopy (SEM), and surface elemental mapping. The electrocatalytic activity for the hydrogen evolution reaction (HER) is evaluated by making electrochemical measurements. In addition, the optimization of the electrodeposition bath is investigated to promote the HER activity. The results show that nickel-molybdenum (1:2) alloy exhibits a higher HER activity, and a current density of 180 mA cm^{-2} is achieved at −1.7 V vs. Ag/AgCl using this coating. Also, the polarization curves of the electrolysis cell demonstrate that using the optimized cathode, the cell operates at 1.9 V at a current density of 1.5 A.cm^{-2} and the operating temperature of 60 °C, which is suitable for use in large-scale industrial AWE units.

Keywords Alkaline water electrolysis · Electrodeposition · Hydrogen evolution reaction · Nickel-molybdenum alloy · Stainless steel

Introduction

Hydrogen as an energy carrier is a promising candidate to store green energy [1]. For hydrogen production, non-renewable sources such as natural gas reforming or renewable sources such as electrolysis can be used [2]. Sources of hydrogen production and distribution can vary according to geographical, climatic, and other characteristics of different regions. In areas where cheap natural gas resources are available, hydrogen production from gas sources is the most cost-effective way [2–4], and in areas where cheap and affordable electricity is available, hydrogen production is justified economically by hydrolysis. Also, ethanol has a particular advantage as a primary source of hydrogen in areas where other fuels are present [5, 6]. It is important to note that among all the different methods of hydrogen production, hydrolysis can be considered a sustainable method if the energy sources used in hydrolysis are provided using renewable sources.

As the electric current flows through water, hydrogen and oxygen are produced. The hydrogen produced by the method mentioned above has high purity, which reaches above 99.99% [7]. The high purity of hydrogen is one of the advantages of electrolysis over the other methods. Among the different technologies for water electrolysis, alkaline water electrolysis (AWE) is a mature technology, and several megawatt electrolysis systems use this technology for hydrogen production around the world [6–8].

Finding inexpensive electrocatalysts and electrodes is considered a major challenge for the hydrogen evolution reaction (HER). The HER mechanism on the metal

Highlights
- The catalytic activity of Ni, Mo, and Ni-Mo alloy–coated stainless steel is compared in the HER.
- Ni-Mo-coated cathode is more active than Ni and Mo coatings for the HER.
- The electrodeposition bath composition affected the catalytic activity of Ni-Mo alloy.
- Optimization of electrodeposition bath leads to an increase in the cathode active area and HER activity.

✉ Mohammad Zhiani
m_zhiani@cc.iut.ac.ir

[1] Department of Chemistry, Isfahan University of Technology, Isfahan 84156-83111, Iran

[2] Department of Chemistry, Tarbiat Modares University, Tehran, P.O. Box 14115-117, Iran

surface in alkaline media can be treated as a combination of three steps [5, 9]:

$$H_2O + e^- + M \rightarrow MH_{ads} + OH^- \text{(Volume reaction)}$$

$$MH_{ads} + H_2O + e^- M + OH^- + H_2 \text{(Heyrovsky reaction)}$$

$$2MH_{ads} M + H_2 \text{(Tafel reaction)}$$

The better electrocatalytic activity of noble metals such as the platinum group metals (PGMs) along with their high price has urged researchers to find a cheap and affordable alternative to the abovementioned metals. The alternatives include non-noble metal catalysts that have moderate electrocatalytic activity for the HER (e.g., nickel, iron, cobalt, and molybdenum and their alloys) [10–13].

The electrocatalyst used in an alkaline medium must have high corrosion resistance, high electrical conductivity, and good catalytic activity. Previous studies have shown that different catalysts are used to accelerate the HER [13]. According to the obtained results, nickel alloying with other metals is one of the most effective ways to improve HER kinetics in AWE [14]. Metals containing more unpaired d electrons (such as molybdenum) have lower d orbital characteristics and can interact with electron donor species more strongly and thus absorb more hydrogen [11, 12]. Several lines of research have shown that nickel-molybdenum alloys are the best catalysts after platinum in terms of activity and function for the HER. Coating nickel-molybdenum alloy on nickel foam increases the electrochemically active surface area, which makes the resulting electrode a promising candidate for use as the cathode of alkaline water electrolyzers. Experimental data have shown that nickel-molybdenum deposition in the sulfate-nickel bath on graphene oxide surface with enhanced active surface contact between substrate and composite promotes the HER [13, 14]. In addition, previous reports have shown that nickel-molybdenum composite coating has more electrochemical activity than nickel-molybdenum alloy. Thus, the composite coating may be useful in the HER applications.

Due to the high activity of nickel for HER and its high stability in alkaline media, this element is considered as one of the most important materials used in alkaline electrolyzers. However, inactivation of the nickel surface due to the formation of nickel hydride and saturation at high concentrations is the main problem of using Ni electrodes. Surface modification and adding molybdenum to increase surface area are some of the modification methods to overcome the inactivity problem [12–14]. Table 1 shows a summary of some research findings on the application of Ni-Mo for the HER in AWE.

According to Table 1, despite the high activity, availability, and economic efficiency of Ni-based coatings and steel substrates, no research has been carried out on the application of Ni-Mo-coated steel optimization for the HER. Thus, the main aim of the present study is the optimization of Ni-Mo-coated stainless steel cathodes for AWE. Some parameters such as electrodeposition current density, pH, and variation of bath composition can affect the cathode efficiency. So, the influence of the abovementioned parameters on electrode surface properties and the HER activity is investigated.

Table 1 A summary of some research on the application of Ni-Mo for the HER in alkaline media

Electrode substrate	Coating composition and bath condition	Research target	Refs
Mild steel	Co-deposition of nickel, iron, and molybdenum (Ni–Fe-Mo) current density of 135 mA cm^{-2} in 6 M KOH solutions at 70 °C	Electrochemical and morphological studies of electrodeposited Ni–Fe-Mo-Zn alloys tailored for water electrolysis	[15]
Steel	Ni-Mo composite current density of 100 mA cm^{-2} in 5 M KOH solution	Electrodeposition of Ni with Mo particles on a steel substrate for HER	[16]
Copper plate	Electrodeposited (NiMo) coatings from a low concentration bath at pH:10	Electrochemical water electrolysis using electrodeposited (Ni-Mo) coatings from a low concentration bath	[17]
Steel	Ni-Mo/WC composites 25 °C and 1 M KOH	Electrocatalytic evaluation of the electrodeposited Ni-Mo/WC composites for HER	[18]
Carbon steel disc	Co–Ni-Mo Current densities of 97 and 87 mA cm^{-2} in 1 M KOH at 25 °C	HER activity of the electrodeposited Co–Ni-Mo, Co–Ni and Co-Mo alloy coatings	[19]
Nickel foam	Ni-Mo alloy current densities of 97 and 87 mA cm^{-2} in 1 M KOH at 25 °C	Influence of electrodeposited Ni-Mo alloy on the HER activity of nickel foam cathode	[20]
Stainless steel	Pd–Ni-Mo 1 M NaOH at 313 K	The HER activity evaluation of Pd–Ni-Mo film as a cathode material	[21]
Copper plate	Ni-Mo alloy current density range of 1.0–4.0 A dm^{-2} in 1 M KOH solution at pH 9.5 and 303 K	Electrodeposition and characterization of Ni-Mo alloy as an electrocatalyst for alkaline water electrolysis	[22]
Steel plate (St3S)	Ni-Mo alloy 5 M KOH solution at pH 9.5 and 293 K	The hydrogen evolution reaction on electrolytic nickel-based coatings containing metallic molybdenum	[23]

Experimental

Preparation of Ni-Mo-Coated Stainless Steel

The plating solution was composed of nickel sulfate ($Ni(SO_4)_2{\cdot}6H_2O$, 0.1 M), sodium molybdenum ($Na_2MoO_4{\cdot}2H_2O$, 0.01 M), tri-sodium citrate ($Na_3C_6H_5O_7{\cdot}2H_2O$, 0.25 M), and boric acid (H_3BO_3, 0.05 M). The molar ratio of nickel to molybdenum was considered to be 2:1. In the electroplating bath, all materials were purchased from Merck, and deionized water was used to make the solutions. The weighted $Ni(SO_4)_2{\cdot}6H_2O$, $Na_2MoO_4{\cdot}2H_2O$, and $Na_3C_6H_5O_7{\cdot}2H_2O$ were 0.42 g, 1.02 g, and 3.6768 g, respectively, for adding to 50 ml deionized water. The pH increased from 8.5 to 9.5 using 0.1 M of NaOH solution, and during electrodeposition, the temperature was set at 25 °C. The coatings were deposited on a piece of 304 stainless steel grid with a dimension of 5 cm^2 and thickness of 0.8 mm. Before electroplating, the electrode substrate was immersed in 5 wt% hydrochloric acid for surface cleaning and, after that [24], it was washed with deionized water several times in an ultrasonic bath. For electroplating, a Pt plate was used as the anode. Electrodeposition was performed by the chronocoulometry method at two potential steps of −0.862 and −1.303 V vs. Ag/AgCl. After reaching the charge of 100 C, the electrodeposition process was stopped.

Characterization of Electrodeposited Coating

The X-ray diffraction (XRD) technique was used to identify the crystal structure of deposits. Philips X'pert MPD diffractometer with a single CuK_α beam and wavelength of 1.5046 Å at 40 kV and 30 mA cm^{-2} current density was applied. Diffraction was performed in the range of 2θ between 0 and 100° with a step of 0.05° and a stop time of 1 s. X'Pert High Score software was used to determine the phases in the sample. Field-emission scanning electron microscope (Quanta FEG-450) was used to investigate the surface morphology of deposited coating on the stainless-steel substrate. The composition of coated films was analyzed by the Octane Elite (Ametek) energy-dispersive X-ray spectrometer coupled to the FE-SEM unit. Also, the element distribution map on the surface of the prepared cathode was evaluated using the Bruker XFlash detector.

Electrochemical Measurements

In order to evaluate the HER activity of the prepared electrodes, a three-electrode configuration was applied using a 1-cm^2 Pt plate and Ag/AgCl electrode as counter and reference electrodes, respectively. It should be noted that a piece of the as-prepared cathode with the dimensions of 1 cm^2 was used as the working electrode. All experiments were carried out in 1 M of KOH at a temperature of 25 °C. Electrochemical measurements were performed using a Sama 500 potentiostat/galvanostat system. Cyclic voltammetry (CV) and linear sweep voltammetry (LSV) measurements were carried out in a potential range of −0.6 to −1.7 V vs. Ag/AgCl and at the scan rate of 50 and 3 mV s^{-1}, respectively. Prior to conducting three-electrode experiments, nitrogen gas was blown into the electrolyte for 30 min at a flow of 50 ml min^{-1}. The purpose of nitrogen blowing is the complete removal of dissolved oxygen in the electrolyte. To evaluate the activity of the prepared cathodes for the HER under real operating conditions of an alkaline water electrolyzer, a membrane electrode assembly (MEA) was prepared and inserted in a 5-cm^2 electrolyzer cell (AHNSCO, Iran). To fabricate an MEA, a 5×5-cm^2 anion exchange membrane A-006 (from Tokuyama) was sandwiched between the prepared cathode and a commercial anode (from Dioxide Materials). In addition, two silicone gaskets with a thickness of 500 µm were used for electrolysis cell sealing. The electrolyzer cell was filled with 4 M of KOH solution 5 h before the cell tests to ensure the complete wetting of the membrane. During the cell tests, 4 M of KOH was injected into the anode and cathode of the cell using a peristaltic pump with a flow rate of 10 ml min^{-1} (Fig. 1). To obtain the polarization curves of the electrolyzer, a chronopotentiometry experiment was performed at the current density range of 0–1500 mA cm^{-2} using an external power supply (Dazheng, PS-305D).

Results and Discussion

Electrochemical Characterization

Activity Evaluation of Different Coatings for HER

Figure 2 represents the 1st and 200th cyclic voltammograms of bare and Ni, Mo, and Ni-Mo-coated stainless steel in the HER potential region. As shown in Fig. 2, the Ni-Mo coating with the HER onset potential of −1.2 V exhibits a higher HER activity. Also, the current density of the mentioned electrode at −1.7 V is 140 mA cm^{-2}, which is higher than that of other electrodes. Compared with the Ni-Mo coating, the bare, Ni, and Mo-coated stainless steel shows a lower HER activity. The onset potential and current density at −1.7 V for the mentioned cathodes are approximately −1.4 V and 70–90 mA cm^{-2}, respectively. To thoroughly evaluate the HER activity of the electrodes, the LSV measurement is used [25, 26].

As shown in Fig. 3, the HER activity of the coatings can be classified into two categories. The best electrochemical

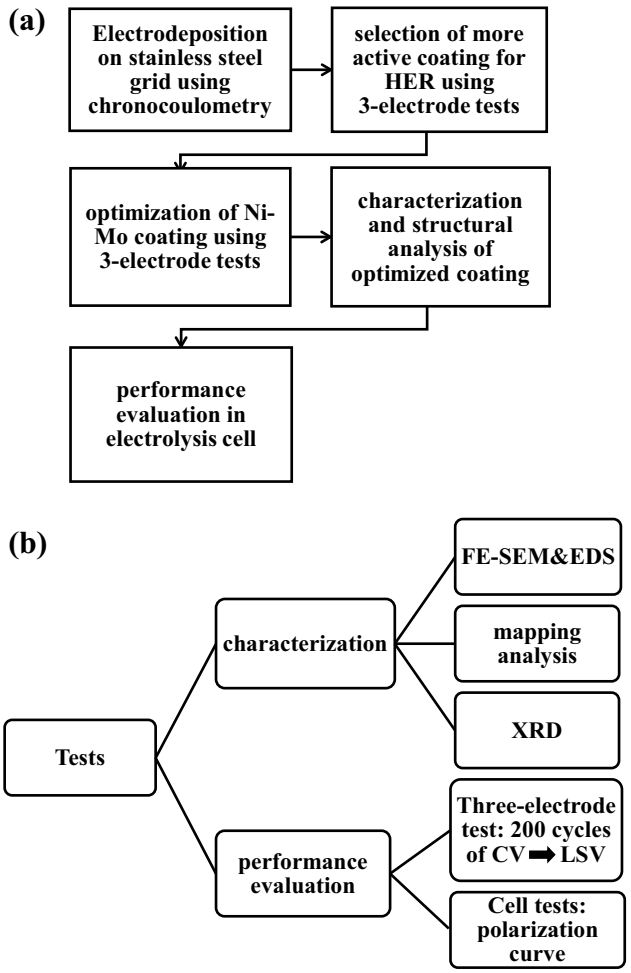

Fig. 1 Flowchart of test steps (**a**) and characterization and performance evaluation tests (**b**)

activity is achieved in the first category with the onset potential of −1.1 V and a high current density of approximately 150 mA cm^{-2} at −1.7 V. Among the deposited coatings, only the nickel-molybdenum alloy falls into the first group. The second group includes nickel, molybdenum, and bare stainless steel. The onset potential of the HER on the second group coatings is approximately −1.4 V, and the current density of 75 to 85 mA cm^{-2} is achieved at −1.7 V. A lower Tafel slope indicates an improvement in the HER kinetics. According to the results of Table 2, electrodeposition on the surface of the stainless-steel grid decreases the Tafel slope in such a way that the amount of the mentioned parameter is reduced from 398 mV dec^{-1} for the bare steel to 122 mV dec^{-1} for the Ni-Mo (1:2) alloy–coated cathode.

The results related to the HER activity obtained from the LSV curves are summarized in Table 2. The mentioned electrochemical values in Table 2 reveal that the Ni-Mo (1:2) alloy coating shows a superior activity compared to the Ni or Mo metallic deposits. In addition, the proper HER activity of the Ni-Mo (1:2) coating retained during 200 cycles of CV is shown in Fig. 3.

As a non-noble metal, nickel has been used for the HER catalysis for a long time. It should be noted that nickel is a 3d transition metal, and its d orbitals are compressed [27–29], so the interaction between nickel and hydrogen atoms is less than 4d and 5d series metals. So, it is necessary to optimize the properties of nickel to fabricate a suitable nickel-based catalyst for the HER [28]. Increasing the catalytic activity of nickel for HER can be provided by preparing binary and ternary nickel alloys. This is because alloying transition metals changes the electron density of valence orbitals and metal fermi levels, thereby changing the M-H bond strength [28, 30]. Alloying left transition metals that have empty or half-filled d-orbitals with a right intermediate metal that has full-filled d-orbital can improve the HER activity [31–33]. The superior and stable activity of the Ni-Mo coating reveals that alloying Ni and Mo increases the contribution of unpaired electron orbitals, which leads to the strengthening of the M-H bond according to the Volmer stage [24, 34]. This phenomenon leads to a decrease in the HER activation energy, which results in a decrease in the onset potential [35]. The optimization of the cathode of the Ni-Mo-coated stainless steel will be investigated in the next section.

Optimization of the Ni-Mo-Coated Stainless Steel

The Effect of Plating Bath pH

Figure 4 a shows that pH increase from 8.5 to 9.5 results in an improvement in the HER activity due to further stabilization of the deposited layer at a pH of 9.5 [24, 28]. As shown in Fig. 4a, at a pH of 9.5, an onset potential of −1.2 V and a current density of 158 mA cm^{-2} is achieved at −1.7 V. At a pH of above 9.5, the nickel precursor tends to precipitate in the nickel hydroxide form rather than electrodeposition on the stainless-steel grid [9, 36]. So, a further increase in pH leads to a reduction in the performance. According to the results, a plating pH of 9.5 is selected for the Ni-Mo electrodeposition.

Effect of Ni-Mo Molar Ratio

Different amounts of Ni and Mo precursors are used in a plating bath to investigate the effect of the Ni-Mo molar ratio on the HER activity. According to Fig. 4b, the 1Ni:2Mo molar ratio shows that a superior HER activity, an onset potential of −1.1 V, and a current density of 186 mA cm^{-2} are obtained using this electrode. As mentioned earlier, alloying Ni and Mo increases the contribution of unpaired electron orbitals, strengthens the M-H bond on the surface of the cathode, and decreases the activation energy. Therefore, the mentioned effect is reduced at high molar ratios

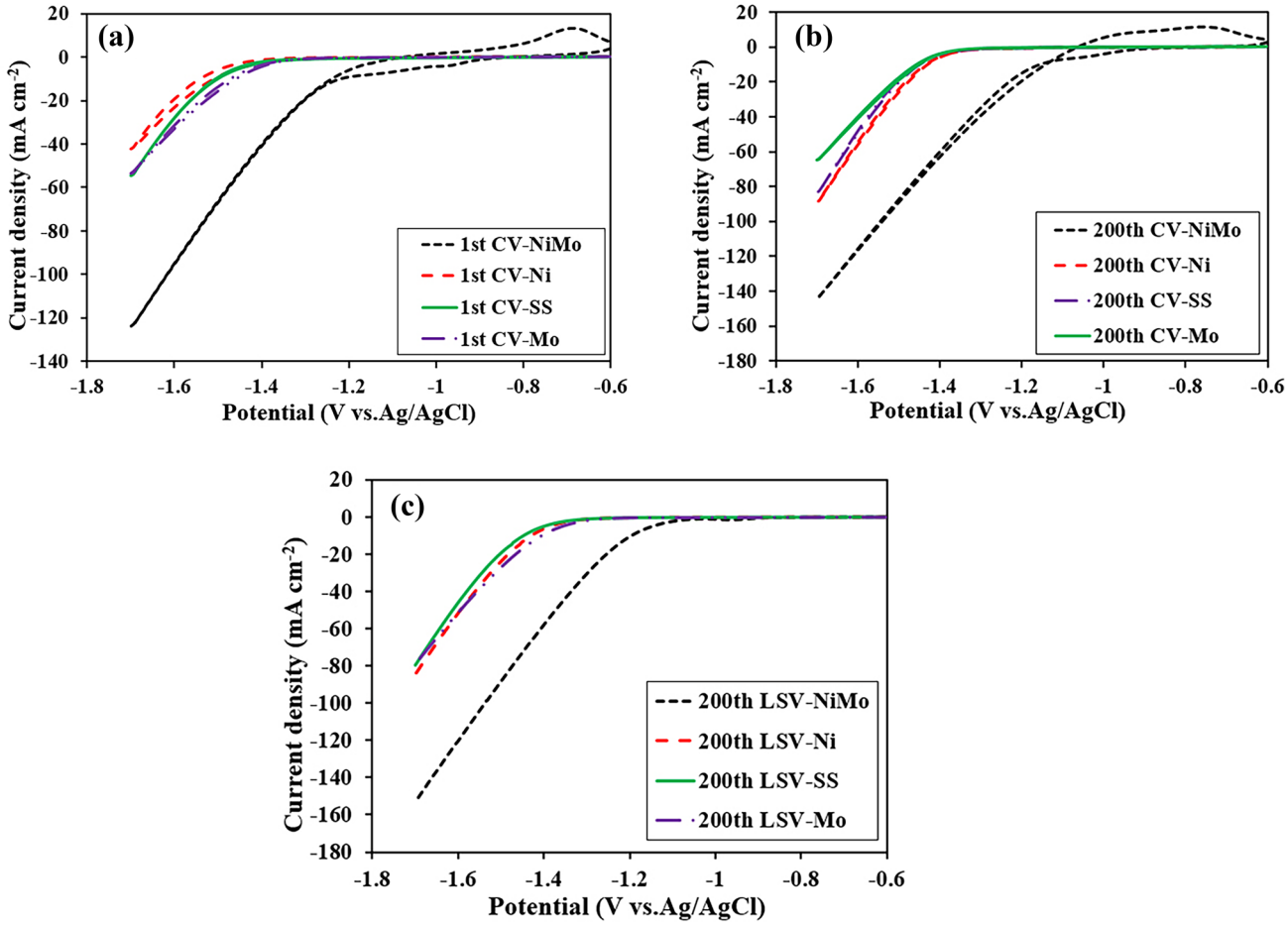

Fig. 2 The 1st and 200th cyclic voltammograms (**a**, **b**) and LSV curves (**c**) of bare and Ni, Mo, and Ni-Mo-coated stainless steel in 1 M KOH

of nickel, which ultimately leads to a decrease in the HER activity. On the other hand, increasing the Mo molar ratio from 2 to 3 reduces the adsorption of hydrogen atoms on the surface of the cathode. Increasing the molar ratio of Mo to higher than the optimum value causes the surface properties of the cathode to deteriorate due to a higher atomic radius of Mo and disruption of the hole-electron balance [15, 37].

Effect of Boric Acid Concentration

The particles are stable as indefinite species in a solution, as confirmed by the appearance of no precipitate when sitting at room temperature for 12 h [37]. Therefore, solutions can be used to deposit the Ni-Mo coatings on the stainless steel. The effect of concentrations of 0.01, 0.03, 0.05, 0.07, and 0.09 molar boric acid in the bath electrodeposited on the stainless steel was investigated by linear sweep voltammetry. At a concentration of 0.05 M, it had a lower onset potential and a higher current density than at other concentrations. Boric acid is a weak acid that acts as a buffer in a plating bath [35, 36]. As can be seen in Fig. 4c, at concentrations below 0.05 M, the pH of the bath is not properly adjusted, resulting in a low HER activity of the prepared electrode. However, since boric acid is a weak acid, a further increase in the concentration of boric acid leads to a decrease in the pH of the plating bath. So, the best HER activity is obtained by using 0.05 M of boric acid.

Effect of Sodium Citrate Concentration

Sodium citrate acts as a complexing agent in an electrodeposition bath that prevents metal salt precipitation and reduces the concentration of free metal ions. Therefore, the concentration of sodium citrate plays an essential role in the properties of the prepared electrode. Figure 4 d shows that the highest HER activity is obtained using 0.25 M of sodium citrate. Increasing the concentration of sodium citrate from 0.15 to 0.25 M by preventing the precipitation of metal ions causes an improvement in the coating surface properties, and as a result, the HER activity increases. However, increasing the concentration of sodium citrate from 0.25 to 0.3 M results in a decrease in the HER

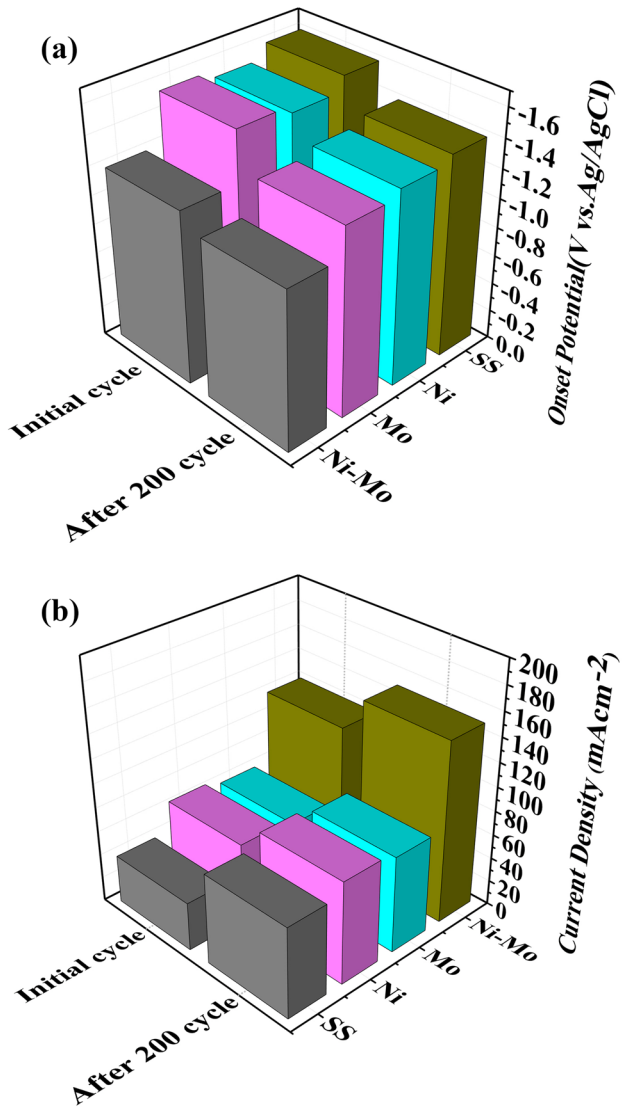

Fig. 3 Diagram of current density at −1.7 V (**a**) and onset potential (**b**) change during 200 cycles of CV

activity. This is because at very high concentrations of the complexing agent, the electrodeposition rate and coating surface properties decrease [38–41].

Comparison of the HER Activity of Ni-Mo Coating During the Optimization Process

After the step-by-step optimization and investigation of the effect of some effective parameters of the electroplating bath (pH, metals molar ratio, as well as the concentration of sodium citrate and boric acid salts), the HER activity of the electrode has improved. The comparative LSV curves before and after the optimization process are shown in Fig. 4e. As can be seen, using the optimized electrode for HER causes the onset potential to change from −1.2 to −1.1 V (vs. Ag/AgCl). In addition, during the optimization process, the current density at −1.7 V is increased by 29%. So, after investigating the structural properties of the optimized cathode, it is necessary to evaluate its performance in single-cell electrolysis to validate its proper performance for large-scale electrolyzers.

Structural Properties of the Optimized Electrode

Figure 5 (a–c) show the surface morphology of the bare and Ni-Mo-coated stainless steel. A comparison of the FE-SEM micrograph illustrates that the rough, compact, and homogeneous Ni-Mo coating covers the smooth surface of the steel grid after the electrodeposition [11, 12]. The elemental mapping is presented in Fig. 5 (d–f) to investigate the distribution of the elements on the surface of the prepared electrode. The distribution of the individual elements shows a uniform distribution of Ni and Mo on the surface of the steel grid. The regular surface structure leads to an improvement in the electrochemical properties and to the development of active sites on the surface of the electrode [40–42]. The uniform distribution of active sites on the surface of the electrode substrate prevents the agglomeration of the catalyst and causes the entire surface of the cathode to be used for HER. It should be noted that according to FE-SEM images, the average thickness of the Ni-Mo coating is 151 nm.

The atomic percentages of Ni, Fe, Cr, and Mo of the prepared electrode are determined based on the EDS analysis and are listed in Table 3. According to the EDS results, the highest contents are related to Fe and Cr, which

Table 2 The obtained electrochemical parameters from LSV for the different coatings and a comparison between the obtained results and the other research results

Cathode coating	Onset potential (V vs. Ag/AgCl)	Tafel slope (mV dec^{-1})	i at −1.4 V (mA cm^{-2})	i at −1.7 V (mA cm^{-2})	Refs
Bare stainless steel	−1.45	398	0	−73	This work
Mo	−1.3	270	−9	−80	This work
Ni	−1.4	161	0	−84	This work
Ni-Mo (1:2)	−1.2	122	−61	−152	This work
Ni-Mo	−1.1	196	-	-	[1]
Ni + Mo (56%:44%)	-	150	-	-	[16]
Ni-Mo	−1.18	-	−60	-	[17]
Ni-Mo	-	208	-	-	[18]
Ni-Mo	−1.02	120	-	-	[22]

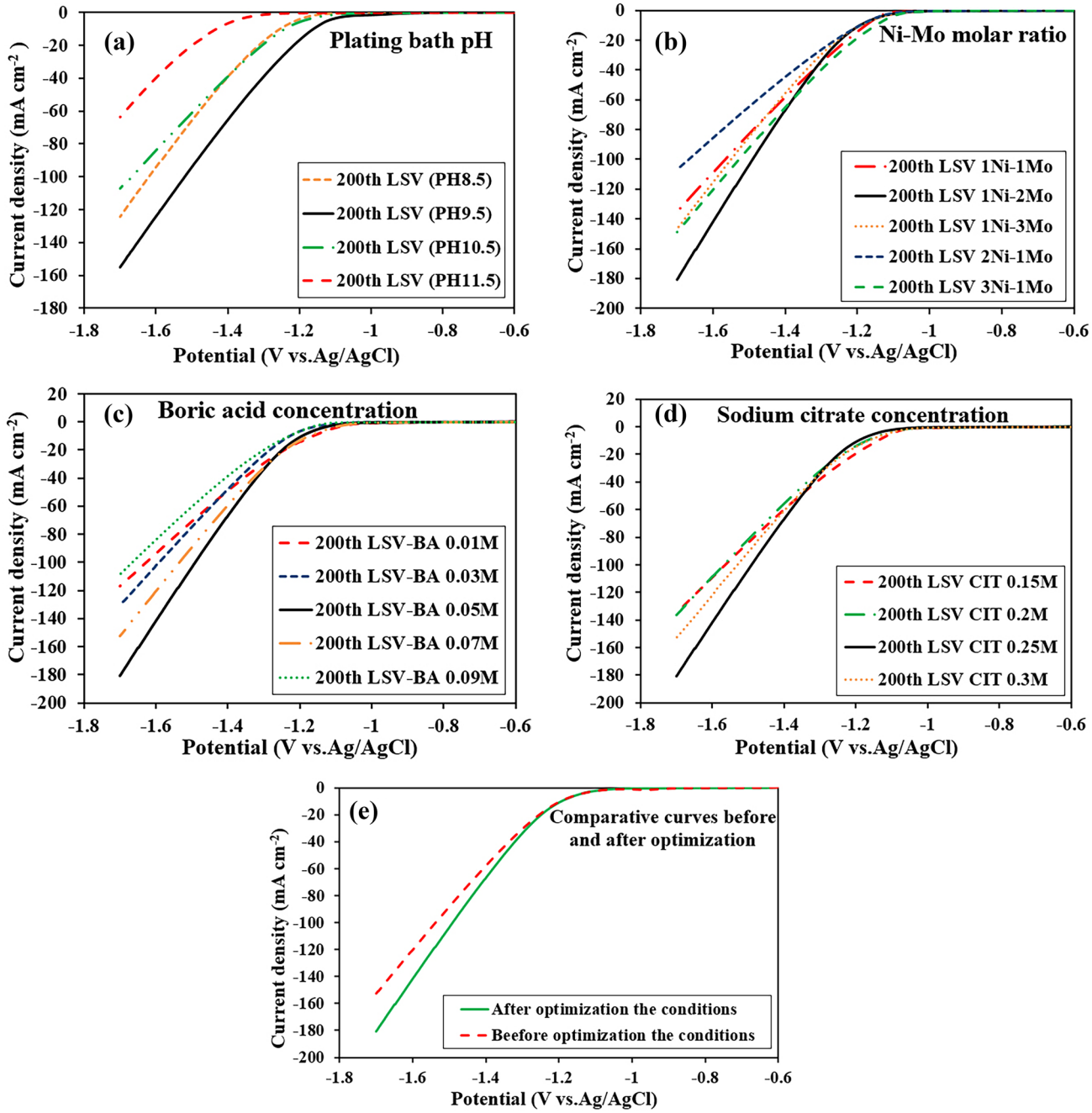

Fig. 4 LSV curves of the Ni-Mo-coated stainless steel during the electrode structure optimization

are present in the steel substrates. Also, the atomic percentages of Ni and Mo are 13.05% and 7.67%, respectively. The higher Ni content is attributed to the presence of Ni in the stainless-steel substrate.

XRD pattern of the prepared electrode is shown in Fig. 6. In this pattern, four characteristic peaks of the Ni cubic structure corresponding to the (111), (200), (220), and (311) planes are visible at 2θ of 43.149°, 50.45°, 74.354°, and 90.285°, respectively. However, in comparison with pure Ni, all the mentioned peaks show peak shifting to lower 2θ values related to the entrance of Mo to the lattice structure of Ni and Ni-Mo alloy formation [41–47].

Performance Evaluation of Optimized Cathode in Alkaline Water Electrolyzer

Electrocatalysts made for use at industrial scales should be evaluated in a simulated environment [45]. For this

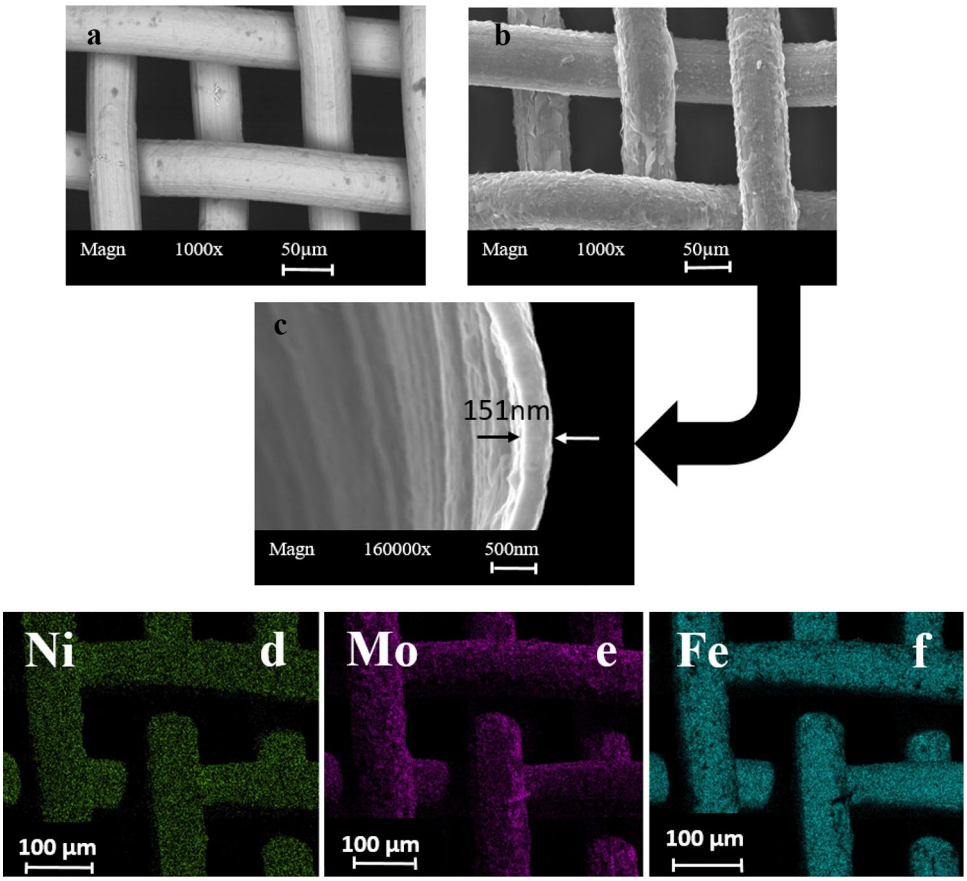

Fig. 5 FE-SEM micrographs of the bare (**a**) and Ni-Mo-coated steel grid (**b**, **c**) and elemental mapping of Ni-Mo-coated steel grid (**d**–**f**)

purpose, a membrane electrolysis cell with an area of 5 cm^2 was prepared. Using a nickel-molybdenum alloy coated on a stainless-steel substrate, an electrocatalyst, and an anion-exchange membrane complex was fabricated by the cell under operating conditions including 4 M of KOH solution, and room temperatures of 40 °C and 60 °C were evaluated.

The polarization curve of a 5-cm^2 cell is recorded at the room temperature, 40 °C, and 60 °C to evaluate the performance of the optimized cathode under actual electrolysis conditions. The results are shown in Fig. 7. As the I-V curves show, with the increase in temperature, the performance of the electrolysis improves in the overall current density regions. For example, while using the optimized cathode, by increasing the temperature from room temperature to 60 °C, the cell voltage at 1 A cm^{-2} is reduced from 2.15 to 1.55 V, which is due to the easier overcome of the activation energy barrier, decrease of ohmic resistance, and improvement of the mass transfer process at higher temperatures [28, 37, 47]. In addition, compared with a bare steel grid, using the optimized cathode causes a decrease in the cell voltage at the same temperature and current density. For example, using the Ni-Mo-coated steel grid at 40 °C, the cell voltage is reduced from 2.6 to 1.75 V. Considering the similarity of the anode and membrane in both electrolysis cells, the observed performance difference is due to the high activity of the Ni-Mo coating for HER. This confirms the obtained results of three-electrode tests and the performance of the optimized hydrogen electrode (Table 4).

Table 3 Chemical composition of the optimized electrode using EDS analysis

Element	Ni	Fe	Cr	Mo
Atomic%	13.05	60.85	18.43	7.67

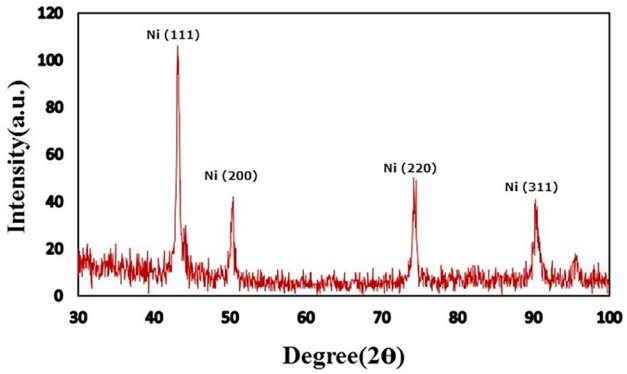

Fig. 6 XRD pattern of Ni-Mo-coated stainless steel grid

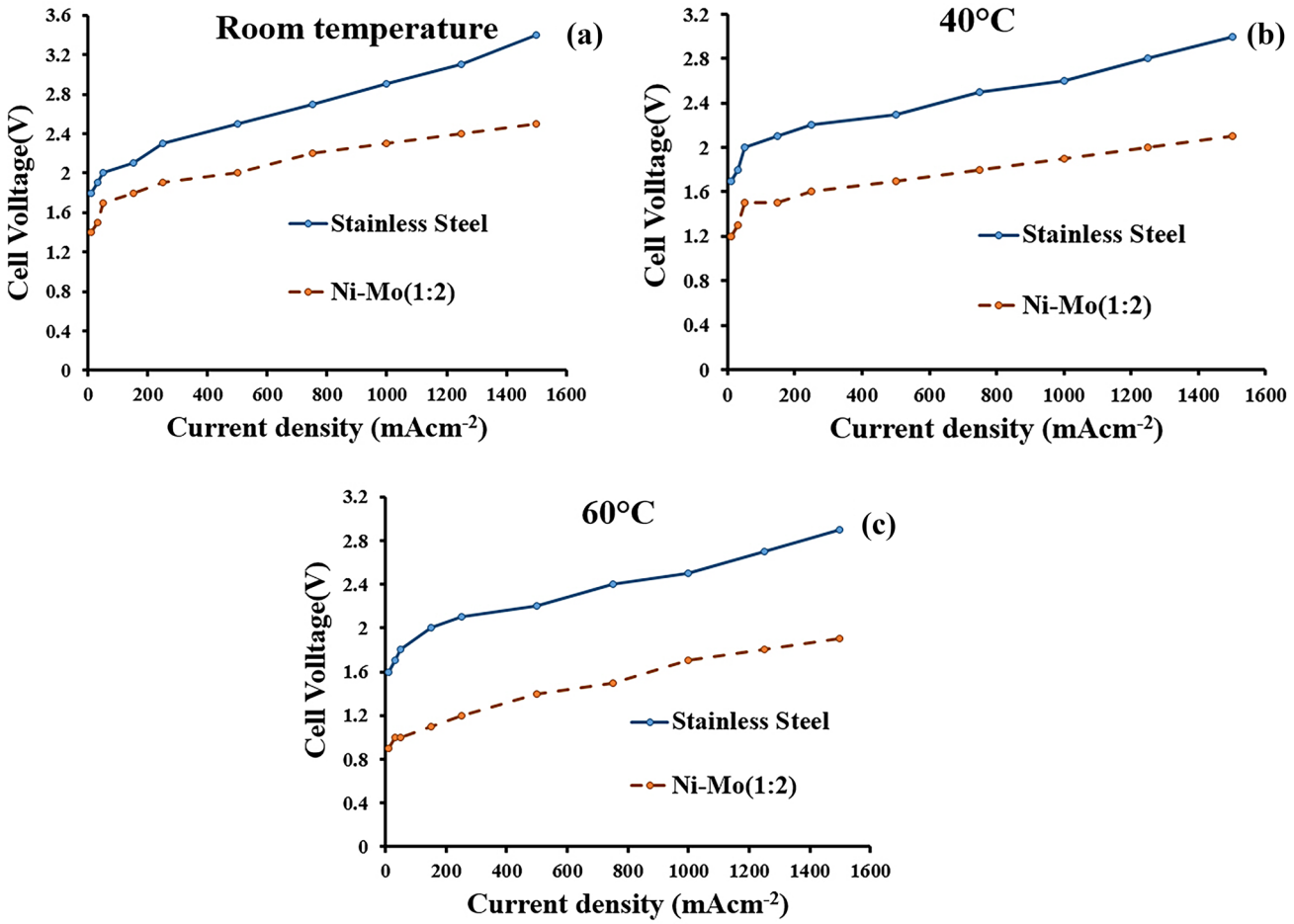

Fig. 7 Polarization curves of alkaline water electrolysis cell using bare and Ni-Mo (1:2)-coated stainless steel cathode at **a** room temperature, **b** 40 °C, and **c** 60 °C

Table 4 The electrolysis cell voltage at different current densities for the bare steel and modified cathodes

Cathode	Cell temperature (°C)	Cell voltage at 0.5 A cm^{-2}	Cell voltage at 1 A cm^{-2}	Cell voltage at 1.5 A cm^{-2}
Bare steel	Room temperature	2.5	2.82	3.4
	40 °C	2.35	2.6	2.92
	60 °C	2.28	2.44	2.83
Modified Ni-Mo-coated steel	Room temperature	1.95	2.15	2.35
	40 °C	1.63	1.75	1.95
	60 °C	1.4	1.55	1.82

Conclusions

The main objective of the present work was to build and optimize a highly active hydrogen electrode using commercially available materials. For this goal, a 304 stainless steel grid was used as the cathode substrate, and Ni-Mo-based coatings were electrodeposited on it. Then, based on the electrochemical measurements, the coating structure was optimized step by step, and finally, it was used as the cathode of an AWE cell. The most important points to summarize are:

1. Ni-Mo alloy coating shows a higher activity than pure Ni and Mo for the HER in alkaline media and retains its activity during 200 cycles of CV.
2. By optimizing the electrodeposition bath parameters and selecting a pH of 9.5, the molar ratio of 1Ni-2Mo, a concentration of 0.05 M for boric acid, and 0.25 M for

sodium citrate in a plating bath, the HER activity of the Ni-Mo coating increases and causes a 29% growth in the HER current density at −1.7 V (vs. Ag/AgCl). Furthermore, the performance evaluation of the optimized cathode in an AWE cell shows its high HER activity, which improves the cell performance in the operating temperature range of electrolysis systems.

3. Characterization studies show the rough and compact morphology of the optimized electrode with a uniform distribution of elements on its surface. In addition, the nickel peaks in XRD pattern shift to lower 2θ, indicating the alloying of the coating structure. All the mentioned factors led to the development of electrochemically active sites on the surface of the stainless steel, and as a result, the HER activity improved.

Acknowledgements The authors are thankful to Isfahan University of Technology (IUT) and Tarbiat Modares University (TMU) for their support and encouraging this work.

Author Contribution M. Zhiani and M. Mohammadi Taghiabadi designed and directed the project; M. H. Bagherabadi performed the experiments; M. Mohammadi Taghiabadi and M. H. Bagherabadi analyzed the obtained results and M. Mohammadi Taghiabadi wrote the article.

Availability of Data and Material Not applicable.

Declarations

Ethics Approval Not applicable.

Human Ethics Not applicable.

Consent to Participate Not applicable.

Consent for Publication Not applicable.

Competing Interests The authors declare no competing interests.

References

1. G. Abuin, R. Coppola, L. Diaz, Ni-Mo alloy electrodeposited over Ni substrate for HER on water electrolysis. Electrocatalysis **10**, 17–28 (2019). https://doi.org/10.1007/s12678-018-0490-2
2. N. Danilovic, R. Subbaraman, D. Strmcnik, A. P. Paulikas, D. Myers, V. R. Stamenkovic, M. Markovic, The effect of noncovalent interactions on the HOR, ORR, and HER on Ru, Ir, and $Ru_{0.50}Ir_{0.50}$ metal surfaces in alkaline environments. Electrocatalysis **3**, 221–229 (2012). https://doi.org/10.1007/s12678-012-0100-7
3. F.H. Saadi et al., Operando synthesis of macroporous molybdenum diselenide films for electrocatalysis of the hydrogen-evolution reaction. ACS Catal **4**(9), 2866–2873 (2014). https://doi.org/10.1021/cs500412u
4. B. Pierozynski, T. Mikolajczyk, Cathodic evolution of hydrogen on platinum-modified nickel foam catalyst. Eectrocatalysis **7**, 121–126 (2016). https://doi.org/10.1007/s12678-015-0290-x
5. D.C. Hong, Y. Tsukakoshi, H. Kotani, T. Ishizuka, K. Ohkubo, Y. Shiota, K. Yoshizawa, S. Fukuzumi, T. Kojima, Mechanistic insights into homogeneous electrocatalytic and photocatalytic hydrogen evolution catalyzed by high-spin Ni(II) complexes with S_2N_2-type tetradentate ligands. Inorg. Chem **57**, 7180–7190 (2018). https://doi.org/10.1021/acs.inorgchem.8b00881
6. H. Tanaka, S. Sugawara, K. Shinohara, T. Ueno, S. Suzuki, N. Hoshi, M. Nakamura, Infrared refection absorption spectroscopy of OH adsorption on the low index planes of Pt. Electrocatalysis **6**, 295 (2015). https://doi.org/10.1007/s12678-014-0245-7
7. J.L. Dempsey, B.S. Brunschwig, J.R. Winkler, H.B. Gray, Hydrogen evolution catalyzed by cobaloximes. Acc. Chem. Res **42**, 1995–2004 (2009). https://doi.org/10.1021/ar900253e
8. H. Müller, M. Metzler, N. Barth, B. Conings, H.G. Boyen, T. Jacob, L.A. Kibler, Electrocatalytic behavior of Pd and Pt nanoislands deposited onto 4,4′-dithiodipyridine SAMs on Au (111). Electrocatalysis **9**, 505 (2018). https://doi.org/10.1007/s12678-018-0467-1
9. B. Pierozynski, T. Mikolajczyk, Hydrogen evolution at catalytically-modified nickel foam in alkaline solution. J. Power Sources **271**, 231–238 (2014). https://doi.org/10.1016/j.jpowsour.2014.07.188
10. I. Katsounaros, W.B. Schneider, J.C. Meier, U. Benedikt, P. Ulrich Biedermann, A.A. Auer, K.J.J. Mayrhofer, Hydrogen peroxide electrochemistry on platinum: towards understanding the oxygen reduction reaction mechanism. Phys. Chem. Chem. Phys **14**, 7384 (2012). https://doi.org/10.1039/C2CP40616K
11. J. Gajdzik, J. Lenz, H. Natter, R. Hempelmann, G.-W. Kohring, F. Gifhorn, M. Manolova, D.M. Kolb, Enzyme immobilisation on self-organised nanopatterned electrode surfaces. Phys. Chem. Chem. Phys **12**, 12604 (2010). https://doi.org/10.1039/c0cp00893a
12. F.X. Felpin, T. Ayad, S. Mitra, Pd/C: an old catalyst for new applications-its use for the Suzuki-Miyaura reaction. Europ. J. Org. Chem **12**, 2679–2690 (2006). https://doi.org/10.1002/ejoc.200501004
13. F. Menegazzo, M. Signoretto, E. Ghedini, G. Strukul, looking for the "dream catalyst" for hydrogen peroxide production from hydrogen and oxygen. Catalysis **9**(3), 251 (2019). https://doi.org/10.3390/catal9030251
14. S.R. Mellsop, A. Gardiner, A.T. Marshall, Spontaneous deposition of iridium onto nickel substrates for the oxygen evolution reaction. Electrocatalysis **7**, 226 (2016). https://doi.org/10.1007/s12678-016-0299-9
15. F.C. Crnkovic, S.A.S. Machado, L.A. Avaca, Electrochemical and morphological studies of electrodeposited Ni–Fe–Mo–Zn alloys tailored for water electrolysis. Int. J. Hydrogen Energy **29**, 249–254 (2004). https://doi.org/10.1016/S0360-3199(03)00212-X
16. J. Panek, A. Budniok, Ni+Mo composite coatings for hydrogen evolution reaction. Interface Anal **40**, 237–241 (2008). https://doi.org/10.1002/sia.2735
17. C.N. Gonsalves, A.C. Hegde, Electrochemical water electrolysis using electrodeposited (NiMo) coatings from a low concentration bath. Chem Data Collections **100697** (2021). https://doi.org/10.1016/j.cdc.2021.100697
18. A. Laszczynska, W. Tylus b, I. Szczygieł, Electrocatalytic properties for the hydrogen evolution of the electrodeposited Ni-Mo/WC composites. Int. J. Hydrogen Energy **4**, 103 (2021). https://doi.org/10.1016/j.ijhydene.2021.04.103
19. A. Laszczynska, I. Szczygieł, Electrocatalytic activity for the hydrogen evolution of the electrodeposited Co-Ni-Mo, Co-Ni and Co-Mo alloy coatings. Int. J. Hydrogen Energy **10**, 181 (2019). https://doi.org/10.1016/j.ijhydene.2019.10.181
20. T. Mikolajczyk, B. Pierozynski, Influence of electrodeposited Ni-Mo alloy on hydrogen evolution reaction at nickel foam cathode. Electrochem. Sci **621–630**, 13 (2018). https://doi.org/10.20964/2018.01.68
21. J. Tang, X. Zhao, Y. Zuo, P. Ju, Y. Tang, Electrodeposited Pd-Ni-Mo film as a cathode material for hydrogen evolution reaction. Electrochim. Acta **1041–1049**, 174 (2015). https://doi.org/10.1016/j.electacta.2015.06.134
22. S. Shetty, M.M.J. Sadiq, D.K, Bhat, A.C. Hegde, Electrodeposition and characterization of Ni-Mo alloy as an electrocatalyst for alkaline

water electrolysis. Electroanal. Chem. **57–65**, 796 (2017). https://doi.org/10.1016/j.jelechem.2017.05.002
23. M. Popczyk, The hydrogen evolution reaction on electrolytic nickel-based coatings containing metallic molybdenum. Materials Sci **636–637**, (2010). https://doi.org/10.4028/www.scientific.net/MSF.636-637.1036
24. L.C. Liu, A. Corma, Metal catalysts for heterogeneous catalysis: from single atoms to nanoclusters and nanoparticles. Chem. Rev **118**(10), 4981–5079 (2018). https://doi.org/10.1021/acs.chemrev.7b00776
25. J. Wang, W.H. Fang, Y. Hu, Y.H. Zhang, J.Q. Dang, Y. Wu, B.Z. Chen, H. Zhao, Z.X. Li, Single atom Ru doping 2H-MoS_2 as highly efficient hydrogen evolution reaction electrocatalyst in a wide pH range. Appl. Catal. B Environ. **298**, 120490 (2021). https://doi.org/10.1016/j.apcatb.2021.120490
26. C.Z. Zhu, Q.R. Shi, S. Feng, D. Du, Y.H. Lin, Single-atom catalysts for electrochemical water splitting. Acs. Energy. Lett **3**(7), 1713–1721 (2018). https://doi.org/10.1021/acsenergylett.8b00640
27. E.P. Alsaç, E. Ülker, S.V.K. Nune, Y. Dede, F. Karadas, Tuning the electronic properties of Prussian blue analogues for efficient water oxidation electrocatalysis: experimental and computational studies. Chemistry-A European Journal **24**, 4856–4863 (2018). https://doi.org/10.1002/chem.201704933
28. X. Lv, Z. Xu, Z. Yan, X. Li, Bimetallic nickel–iron-supported Pd electrocatalyst for ethanol electrooxidation in alkaline solution. Electrocatalysis **2**(2), 82–88 (2011). https://doi.org/10.1007/s12678-011-0044-3
29. J. Zhang, PEM fuel cell electrocatalysts and catalyst layers (Springer-Verlag, London, 2008), p.631
30. J.G. Kleingardner, B. Kandemir, K.L. Bren, Hydrogen evolution from neutral water under aerobic conditions catalyzed by cobalt microperoxidase-11. J. Am. Chem. Soc **136**, 4–7 (2014). https://doi.org/10.1021/ja406818h
31. M.A. Khan, H.B. Zhao, W.W. Zou, Z. Chen, W.J. Cao, J.H. Fang, J.Q. Xu, L. Zhang, J.J. Zhang, Recent progresses in electrocatalysts for water electrolysis. Electro. Ener. Rev **1**, 483–530 (2018). https://doi.org/10.1007/s41918-018-0014-z
32. M.L. Helm, M.P. Stewart, R.M. Bullock, M.R. DuBois, D.L. DuBois, A synthetic nickel electrocatalyst with a turnover frequency above 100,000 s−1 for H_2 production. Science **333**, 863–866 (2011). https://doi.org/10.1126/science.1205864
33. P.A. Jacques, V. Artero, J. Pécaut, M. Fontecave, Cobalt and nickel diimine-dioxime complexes as molecular electrocatalysts for hydrogen evolution with low overvoltages. PNAS **106**, 20627–20632 (2009). https://doi.org/10.1073/pnas.090777510
34. V. Artero, J.M. Saveant, Toward the rational benchmarking of homogeneous H_2-evolving catalysts. Energy Environ. Sci **7**, 3808–3814 (2014). https://doi.org/10.1039/C4EE01709A
35. C.N. Lin, D. Xue, Y.H. Zhou, S.Z. Zhan, C.L. Ni, The effect of oxidation state of metal on hydrogen production electro-catalyzed by nickel complexes supported by maleonitriledithiolate ligand. J. Electroanal. Chem **785**, 58–64 (2017). https://doi.org/10.1016/j.jelechem.2016.12.011
36. S. Tuomi, A. Santasalo-Aarnio, P. Kanninen, T. Kallio, Hydrogen production by methanol–water solution electrolysis with an alkaline membrane cell. J. Power Sources **229**, 32–35 (2013). https://doi.org/10.1016/j.jpowsour.2012.11.131
37. A.A. Daryakenari, D. Hosseini, M.H. Mirfasih, A. Apostoluk, C.R. Müller, J.-J. Delaunay, Formation of NiO nanoparticle-attached nanographitic flake layers deposited by pulsed electrophoretic deposition for ethanol electro-oxidation. J. Alloys Compd **698**, 571–576 (2017). https://doi.org/10.1016/j.jallcom.2016.12.136
38. S.S. Jayaseelan, T. Ko, S. Radhakrishnan, C. Yang, H.-Y. Kim, B. Kim, Novel MWCNT interconnected $NiCo_2O_4$ aerogels prepared by a supercritical CO_2 drying method for ethanol electrooxidation in alkaline media. Int. J. Hydrog. Energy **41**(31), 13504–13512 (2016). https://doi.org/10.1016/j.ijhydene.2016.05.175
39. M. Fleischmann, K. Korinek, D. Pletcher, The oxidation of organic compounds at a nickel anode in alkaline solution. J. Electroanal. Chem. Interfacial Electrochem **31**(1), 39–49 (1971). https://doi.org/10.1016/S0022-0728(71)80040-2
40. J. Li, A. Oudriss, A. Metsue, J. Bouhattate, X. Feaugas, Anisotropy of hydrogen diffusion in nickel single crystals: the effects of self-stress and hydrogen concentration on diffusion. Sci. Rep. **7**(45041) (2017). https://doi.org/10.1038/srep45041
41. K. Hashimoto et al., The use of renewable energy in the form of methane via electrolytic hydrogen generation. Appl. Surface Science **388**, 608–615 (2016). https://doi.org/10.1016/j.apsusc.2016.02.130
42. Y. Yu, H. Li, H. Wang, X.Z. Yuan, G. Wang, M. Pan, J. Power Sources **205**, 10–23 (2012)
43. H. Vandenborre, P. Vermeiren, R. Leysen, Hydrogen evolution at nickel sulphide cathodes in alkaline medium. Electrochim. Acta **29**(3), 297–301 (1984). https://doi.org/10.1016/0013-4686(84)87065-6
44. R. Kowalik et al., Electrochemical deposition of Mo-Se thin films. ECS Trans. **24**, 120–127 (2015). https://doi.org/10.1149/06429.0023ecst
45. N. Tkachenko, Electrodeposition of cobalt–tungsten alloys and their application for surface engineering. Russian J. Electrochemistry **52**, 1041–1047 (2016). https://doi.org/10.1134/S1023193516110136
46. U.A. Paulus, A. Wokaun, G.G. Scherer, T.J. Schmidt, V. Stamenkovic, N.M. Markovic, P.N. Ross, Oxygen reduction on high surface area Pt-based alloy catalysts in comparison to well defined smooth bulk alloy electrodes. Electrochim. Acta **47**, 3787–3798 (2002). https://doi.org/10.1016/S0013-4686(02)00349-3
47. M.B. Stevens, C.D.M. Trang, L.J. Enman, J. Deng, S.W. Boettcher, Reactive Fe-sites in Ni/Fe (oxy)hydroxide are responsible for exceptional oxygen electrocatalysis activity. J. Am. Chem. Soc **139**, 11361–11364 (2017). https://doi.org/10.1021/jacs.7b07117

Publisher's Note Springer Nature remains neutral with regard to jurisdictional claims in published maps and institutional affiliations.

Springer Nature or its licensor (e.g. a society or other partner) holds exclusive rights to this article under a publishing agreement with the author(s) or other rightsholder(s); author self-archiving of the accepted manuscript version of this article is solely governed by the terms of such publishing agreement and applicable law.